AGU PUBLICATIONS

JGR

Journal of Geophysical Research: Biogeosciences

RESEARCH ARTICLE
10.1002/2014JG002719

Key Points:
- Summer CDOM loss exceeds short-term variation by an order of magnitude
- Absorption spectral shapes suggest dominance of photochemical decay
- CDOM in a eutrophic, humic lake is unaffected by in-lake DOC production

Supporting Information:
- Text S1, Table S1, and Figures S1–S4

Correspondence to:
R. A. Müller,
roger.muller@ebc.uu.se

Citation:
Müller, R. A., D. N. Kothawala, E. Podgrajsek, E. Sahlée, B. Koehler, L. J. Tranvik, and G. A. Weyhenmeyer (2014), Hourly, daily, and seasonal variability in the absorption spectra of chromophoric dissolved organic matter in a eutrophic, humic lake, *J. Geophys. Res. Biogeosci.*, *119*, 1985–1998, doi:10.1002/2014JG002719.

Received 31 MAY 2014
Accepted 28 AUG 2014
Accepted article online 4 SEP 2014
Published online 16 OCT 2014

Hourly, daily, and seasonal variability in the absorption spectra of chromophoric dissolved organic matter in a eutrophic, humic lake

R. A. Müller[1], D. N. Kothawala[1], E. Podgrajsek[2], E. Sahlée[2], B. Koehler[1], L. J. Tranvik[1], and G. A. Weyhenmeyer[1]

[1]Department of Ecology and Genetics/Limnology, Evolutionary Biology Centre, Uppsala University, Uppsala, Sweden, [2]Department of Earth Sciences, Uppsala University, Uppsala, Sweden

Abstract The short-term (hourly and daily) variation in chromophoric dissolved organic matter (CDOM) in lakes is largely unknown. We assessed the spectral characteristics of light absorption by CDOM in a eutrophic, humic shallow mixed lake of temperate Sweden at a high-frequency (30 min) interval and during a full growing season (May to October). Physical time series, such as solar radiation, temperature, wind, and partial pressures of carbon dioxide in water and air, were measured synchronously. We identified a strong radiation-induced summer CDOM loss (25 to 50%) that developed over 4 months, which was accompanied by strong changes in CDOM absorption spectral shape. The magnitude of the CDOM loss exceeded subhourly to daily variability by an order of magnitude. Applying Fourier analysis, we demonstrate that variation in CDOM remained largely unaffected by rapid shifts in weather, and no apparent response to in-lake dissolved organic carbon production was found. In autumn, CDOM occasionally showed variation at hourly to daily time scales, reaching a maximum daily coefficient of variation of 15%. We suggest that lake-internal effects on CDOM are quenched in humic lake waters by dominating effects associated with imported CDOM and solar exposure. Since humic lake waters belong to one of the most abundant lake types on Earth, our results have important implications for the understanding of global CDOM cycling.

1. Introduction

Surface waters receive large amounts of chromophoric dissolved organic matter (CDOM) from terrestrial ecosystems [*Rasmussen et al.*, 1989; *Dillon and Molot*, 1997]. In surface waters, CDOM can have a strong influence on the absorption characteristics of natural waters, thereby influencing a large variety of physical and biological aspects of lake ecology [*Thurman*, 1985]. CDOM affects, for example, the distribution of heat in the water column [*Fee et al.*, 1996; *Snucins and Gunn*, 2000], determines the depth of the photic zone that is important for primary production [*Kirk*, 1994], and restricts the penetration of UV radiation that may harm aquatic organisms [*Morris et al.*, 1995; *Hargreaves*, 2003]. In the visible wave band region, CDOM also affects the color of water which is highly relevant for water quality related issues [*Wetzel*, 1983; *Williamson et al.*, 1999]. Where water bodies are used for drinking water purposes, CDOM concentrations need to be below a threshold value, which can be technically challenging and expensive to achieve [*Siddiqui et al.*, 1997; *Wilhelm*, 2009].

CDOM is typically measured as the light absorption of water after filtration, which excludes interferences from particles [*Kirk*, 1994]. In surface waters, CDOM generally correlates well with dissolved organic carbon (DOC) concentrations, which has been shown on broad sets of samples from flowing waters [e.g., *Tipping et al.*, 2009], lakes [e.g., *Meili*, 1992], and coastal waters [e.g., *Mattson et al.*, 1974; *Green and Blough*, 1994]. There is however a substantial residual variability in CDOM that is not explained by DOC concentrations [*Lean*, 1998]. Variations in CDOM/DOC ratios in freshwaters have previously been attributed to variations in CDOM/DOC imports from soils including the presence and absence of iron [*Shapiro*, 1966; *Kritzberg and Ekström*, 2012; *Weyhenmeyer et al.*, 2014], photodegradation [*Kirk*, 1994; *Graneli et al.*, 1996], flocculation [*von Wachenfeldt and Tranvik*, 2008], and autochthonous production [*Jones*, 1998; *Steinberg*, 2003]. Changing DOC concentrations and variations in CDOM/DOC ratios therewith occur at various temporal (e.g., hourly, daily, and seasonal) scales.

Strong CDOM variability at hourly to subhourly time scales can be observed in flowing waters (headwaters, streams, and rivers) and results from highly variable runoff [e.g., *Jeong et al.*, 2012]. Such short time scales

are poorly detected by manual sampling [*Kirchner et al*., 2004], a reason why deployable spectrophotometric probes have been shown to be powerful devices to capture short-term variability [e.g., *Saraceno et al*., 2009]. Applying high-frequency measurement techniques, *Spencer et al*. [2007] observed a diurnal CDOM signal in a eutrophic river that they attributed to internal DOC production following day-night cycles. Studies that quantify short-term CDOM variability in lakes remain rare. The few available studies measuring at high-frequency intervals indicate that CDOM variations follow in-lake production (macrophyte, phytoplankton, or algae blooms) [*Coloso et al*., 2011; *Liu et al*., 2013], as well as physical processes that include weather [*Jennings et al*., 2012], and interactions with the sediment carbon pool [*Downing et al*., 2008]. However, none of these high-frequency studies have retrieved CDOM measurements at multiple wavelengths and over a whole season. Hence, no direct comparison between hourly, daily, and seasonal variability in the absorption spectra of CDOM is available.

Some monitoring programs have included the absorption measurements at one wavelength (e.g., 420 nm) into their routine analysis [*Erlandsson et al*., 2012]. However, the analysis of CDOM at a single wavelength fails to take advantage of the information contained in the shape of the full absorption spectrum [*Korshin et al*., 1997]. For example, the spectral slope [*Helms et al*., 2008; *Twardowski et al*., 2004] and even the simple absorption ratio of two wavelengths have been successfully linked to biodegradability of DOC [*Berggren et al*., 2007], molecular weight of DOC compounds [*Peuravuori and Pihlaja*, 1997], and photodegradation [*Twardowski and Donaghay*, 2002]. During photodegradation, the incoming solar radiation is absorbed by CDOM and results in changes of the CDOM spectral shape [*Loiselle et al*., 2009]. The molecular composition and spectral characteristics of DOC may be altered either directly through complete photooxidation or indirectly through enhanced bioavailability [*Bertilsson and Tranvik*, 2000]. These spectral metrics are therefore often referred to as indicators of DOC quality [*Erlandsson et al*., 2012] and are more robust to fluctuations in DOC concentrations than measurements of CDOM absorption at one single wavelength [*Loiselle et al*., 2009]. This makes the attempt to quantify CDOM absorption at multiple wavelengths a valuable undertaking.

The overall aim of this study is to assess if the temporal variability in the CDOM absorption spectrum (254 nm to 420 nm) is greatest at short (hourly and daily) or long (seasonal) time scales. Furthermore, we attempt to discern if variations in CDOM absorption are coupled to physical processes. To do this, we measured CDOM at high frequency using an in situ spectrophotometer probe over a whole growing season from May to October of 2011. The study was performed in a shallow humic eutrophic lake where we expect complex physical and biological interactions to influence lake CDOM variability (see above). We deployed the spectrophotometer probe in the lake near a meteorological field station, which recorded physical variables synchronously (solar radiation, wind, temperature, and partial pressure of carbon dioxide (pCO_2)). Finally, we applied Fourier transform analysis, a method commonly used by climatologists, to identify frequencies at which physical variables fluctuate most strongly to disentangle their influence on CDOM variability at hourly, daily, and seasonal time scales.

2. Materials and Methods

2.1. Study Lake

Data were collected from lake Tämnaren (60°10′N, 17°20′E), a shallow humic lake of 36.7 km^2 area in Sweden (Figure 1a). The lake was drained in the 1870s and the 1950s to gain agricultural land, resulting in today's average water depth of 1.3 m [*Wallsten*, 1974; *Brunberg and Blomqvist*, 1998]. The lake catchment is 693.5 km^2 with 61% mixed forest, 24% agricultural land, 9% wetlands, and 6% open waters. The average discharge at the lake outlet is 3.5 $m^3 s^{-1}$ (Swedish Meteorological and Hydrological Institute (SMHI)). A yearly discharge maximum is reached after snowmelt. The average theoretical water retention time is 110 days [*Brunberg and Blomqvist*, 1998]. The historical lowering of the water table stimulated growth of the aquatic vegetation that includes *Phragmites australis* (Cav.) Trin., *Scirpus lacustris* L., *Nuphar luteum* Sm., and *Potamogeton natans* L. along the littoral regions and *Elodea Canadensis* Michx. at more remote parts of the lake. In recent years, *Phragmites australis* (Cav.) Trin. has spread and currently covers an approximate area of 3 km^2 (8.2% of the lake area) along the shores. The lake water quality monitoring by the Swedish University of Agricultural Sciences indicates that Tämnaren is eutrophic, with total phosphorus concentrations of 40 $\mu g L^{-1}$, total nitrogen concentrations of 705 $\mu g L^{-1}$, DOC concentrations of 18.5 mg C L^{-1}, and total iron concentrations of 308 $\mu g L^{-1}$ (medians from autumn surface water samplings in 1995, 2000, and 2005).

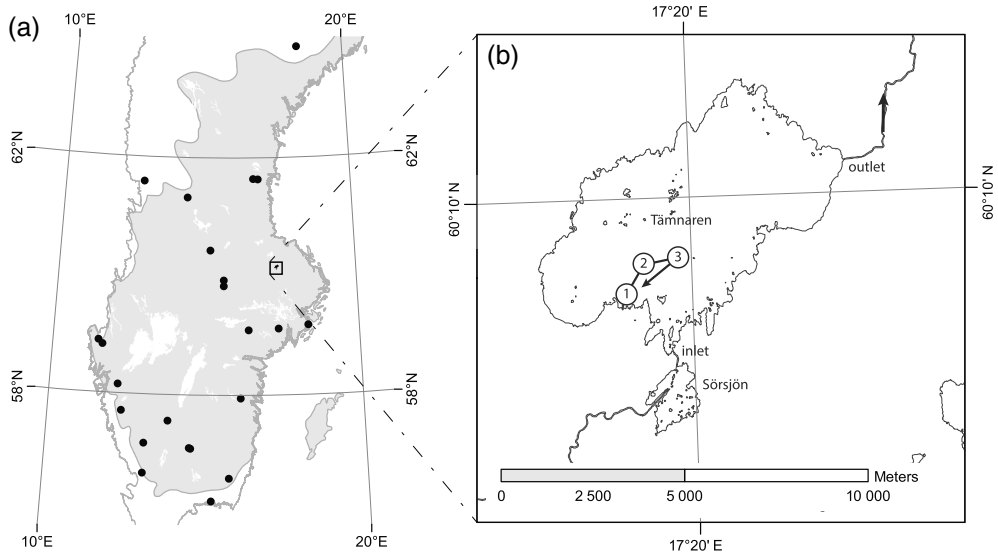

Figure 1. (a) Location of Tämnaren (black square), lakes from the Swedish University of Agricultural Sciences' monitoring database ($N = 23$, black circles), and air temperature zones with mean daily air temperatures above 0°C during 180 ± 20 d yr^{-1} (light grey). (b) Lake Tämnaren with Sörsjön, flow direction, and sampling locations marked as (1) littoral area, (2) sampling site 2, and (3) float with spectrophotometer probe.

2.2. High-Frequency Measurements

The monitoring site was located in the central part of the lake (Figure 1b) and consisted of a float of 3.5 m × 2.0 m in size. In addition, a meteorological tower of 6 m in height was positioned on a small island (20 m × 10 m) at approximately 70 m distance from the float. Monitoring was conducted for the period of 6 May to 19 October 2011. In situ measurements of CDOM were made using a two-beam 256 pixel UV–visible (VIS) spectrophotometer probe with a Xenon light source (spectro::lyser, s-can, Vienna, Austria) that measures beam attenuation at wavelengths from 240 to 735 nm, at 2.5 nm intervals, and across an optical path length of 0.035 m. Values at 254 nm were estimated by linear interpolation between the closest two readings. The probe was attached to the float at a depth of 0.5 m below the water surface and measured at a 30 min interval. Automated cleaning with pressured air (1 s at 5 bar, every 6 h) reduced biofilm growth on the optical windows and kept them free from debris. In addition, the optical windows were cleaned manually at biweekly intervals by applying an environmentally certified cleaning agent (composition: 0.5 to 0.6% K_3PO_4, 0.2 to 0.3% $C_6H_6NNa_3O_6$, $<$0.01% KOH). Automated and manual cleaning combined kept instrument drifts below 1%, as tested by manual measurements in distilled water before and after cleaning, and therefore, a drift correction was not necessary. Automated cleaning failed during the periods of 21 June to 19 July and 24 July to 2 August, and we therefore excluded the respective data from our analysis. Also, spectra retrieved during brief maintenance periods were excluded, resulting in a final data set of 6145 raw spectra. Samples were used as calibration reference to correct raw spectra for particle interferences (see section 2.3).

Water temperature was measured at 0.5 m depth at a 30 min interval using copper-constantan thermocouples (In Situ Instruments, Ockelbo, Sweden). For the periods of 12 May to 17 May 2011 and 24 August to 19 October 2011, partial pressures of carbon dioxide (pCO_2) were measured 0.5 m below the water surface at a 30 min interval using a SAMI sensor (Submersible Autonomous Moored Instrument, Sunburst Sensors, Missoula, MT, USA). At the meteorological tower, air temperature was measured at 1.4 m above ground and at a 1 min interval using radiation-shielded and ventilated thermocouples. Solar radiation was measured as total shortwave (300 to 1000 nm) radiation, 1.5 m above ground and at a 1 min interval using a CS300 Apogee Silicon pyranometer (Campbell Scientific Inc., Logan, UT, USA). Wind was measured at 1.4 m above ground and at a 1 min interval using a propeller anemometer (Young, Traverse City, MI, USA). Atmospheric pCO_2 was measured at 4.7 m above ground at 10 Hz using a LI-7500A open path gas analyzer (LI-COR Inc., Lincoln, NE, USA).

Using the software MATLAB® 7.0.1 (The MathWorks, Natick, MA, USA, 2004), all time series were aligned to 30 min means. Fourier transform analysis was applied to transform high-frequency data (in situ CDOM

measurements and physical time series) from the time domain to the frequency domain, i.e., expressing the data by a sum of sine and cosine terms of different frequencies. We then studied the resulting power spectra for analysis of how much different temporal scales contribute to the total observed variation of the data series (see, e.g., *Stull* [1988] for how this approach is used with meteorological data). Atmospheric pCO_2 (discontinuous time series) was excluded from Fourier analysis. Coefficients of variation (CVs) were calculated for the full CDOM signal as the standard deviation from the mean divided by the mean. CVs for CDOM signals with a return period of once per week and higher (CV_{7D}) were calculated accordingly after the removal of frequencies lower than the weekly signal. CVs for CDOM signals with a return period of once per day and higher (CV_{1D}) were calculated after the removal of frequencies lower than the daily signal. For this purpose, running mean-based frequency filters were applied. In addition, diurnal patterns were analyzed on a 30 min basis and on normalized data, referred to as z-scores [*Quinn and Keough*, 2002]. The normalization was done for each Julian day ($N = 167$) to remove differences in daily means and standard deviations across days.

2.3. Discrete Water Sampling and Laboratory Analyses

Three sites were sampled and are referred to as (1) littoral area, (2) sampling site 2, and (3) float (Figure 1b). Sampling was conducted from 13 May to 19 October 2011 over 21 occasions. On each sampling occasion, we collected one 40 mL headspace-free vial at each site for dissolved inorganic carbon (DIC) analysis. DIC analysis was conducted using a Sievers 900 total organic carbon analyzer (General Electric Analytical Instruments, Boulder, CO, USA) with a detection limit of <0.1 mg C L^{-1}. One 250 mL sample was collected in a polyethylen bottle at the float for Chlorophyll *a* (Chl *a*) analysis. For analysis, cells were collected on glass microfiber filters (Whatman, GF/C), and Chl *a* was extracted with ethanol (95%, 5 min at 75°C). The extract's absorption at 665 and 770 nm was measured and the final values for Chl *a* corrected for pheophytin (International Organization for Standardization (ISO) 1992). In addition, 100 mL samples were collected in polyethylene bottles at each site, with the float sampled in triplicate. This subset of samples was analyzed for turbidity, DOC, and spectral analysis. Turbidity was measured using a HACH® turbidimeter (model 2100P ISO, Loveland, CO, USA), blank subtracted using distilled water, and reported in Nephelometric Turbidity Units (NTU). DOC was measured after filtration (0.45 μm regenerated cellulose, Sartorius) using the total organic carbon analyzer and blank subtracted using distilled water. Using a UV–VIS spectrophotometer (Lambda 45, Perkin Elmer, Norwalk, CT, USA), spectral analysis was run from 200 to 750 nm, at a 1 nm interval, and across an optical path length of 0.01 m (quartz cuvette) before and after filtration (0.45 μm regenerated cellulose, Sartorius). Samples were blank subtracted using the absorption spectra of distilled water.

CDOM was reported as Napierian absorption coefficients $a(\lambda)$ defined following *Kirk* [1994] and *Hu et al*. [2002]:

$$a(\lambda) = A(\lambda) \times ln\,(10) \times L^{-1} \quad (1)$$

where $A(\lambda)$ is the absorbance measured at wavelength λ (dimensionless) on filtered (regenerated cellulose 0.45 μm, Sartorius) samples, $ln(10)$ is the natural logarithm of 10, and L is the optical path length (m). The in situ spectrophotometer probe reports beam attenuation $c(\lambda)$ (m^{-1}), which is subject to additional light losses $n(\lambda)$ that result from interferences with particles [*Kirk*, 1994]:

$$c(\lambda) = a(\lambda) + n(\lambda) \quad (2)$$

Napierian absorption coefficients $a(\lambda)$ measured on filtered samples were used as calibration reference to correct $c(\lambda)$ for $n(\lambda)$ estimating $a(254)$, $a(365)$, and $a(420)$ at high-frequency intervals. For this purpose, generalized linear models were built (Table S1 in the supporting information) using the software JMP® 10.0 (SAS Institute, Inc., Cary, NC, 2010). Running an initial model calibration, we identified samples from 29 September to lie outside a 99% confidence interval. These samples ($N = 3$) were excluded for model calibration. However, model performance was tested on the full sample data set ($N = 54$; Figure S1 in the supporting information). The commonly used absorption ratio, $a(254)/a(365)$, was used as a simple means of evaluating the linear slope between two wavelengths. A lower absorption ratio can be indicative of DOC with higher molecular weight [*De Haan*, 1993; *Dahlén et al*., 1996]. In addition, higher values of the absorption ratio have been related to greater bioavailability [*Berggren et al*., 2007]. Running spectral analysis on both filtered and unfiltered sample volumes, we quantified $a(\lambda)$ and $c(\lambda)$ for the samples (Figure 2a) and determined the wavelength-dependent $a(\lambda)/n(\lambda)$ ratio (Figure 2b). At 730 nm, $a(730)$ was close to zero,

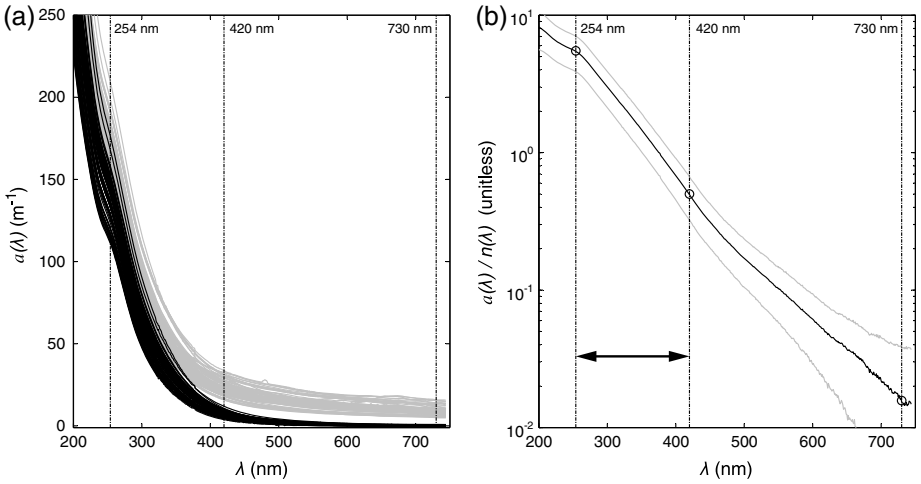

Figure 2. Results from spectral analysis on filtered and unfiltered samples, for 200 to 735 nm, at a 1 nm interval with (a) absorption coefficients $a(\lambda)$ (black), and $c(\lambda)$ (light grey), (b) wavelength-dependent mean for $a(\lambda)/n(\lambda)$ ratio (black line) with standard deviations around the mean (grey lines). The ratio $a(\lambda)/n(\lambda)$ at 254 nm (5.5), 420 nm (0.5), and 730 nm (<0.05) is marked (black circles). The wavelength interval addressed in this study (254 to 420 nm) is marked (black arrow).

and $c(730)$ was near equal to $n(730)$ (equation (2)). Based on these observations, we concluded that the attenuation at 730 nm was strongly dominated by particles, and we decided to report $n(730)$ to discuss temporal variability patterns of interferences from particles.

Specific ultraviolet and specific visible absorption was reported as $a(254)$ and $a(420)$ per unit DOC. The metric $a(254)$ per unit DOC can be converted to the frequently applied metric specific ultraviolet absorbance [*Weishaar et al*., 2003] by division through $ln(10)$. Using MATLAB® 7.0.1, absorption spectral slope distributions $S(\lambda)$ were calculated based on $a(\lambda)$ measured on samples following *Loiselle et al*. [2009]. In brief, $S(\lambda)$ was estimated for each wavelength λ (210 to 330 nm) with 20 nm wavelength intervals applying an exponential function. Fluorescence was measured on filtered samples using a fluorescence spectrophotometer (Fluoromax 2, Horiba Jobin Yvon, New Jersey, USA). Spectra were measured using a 1 cm^2 quartz cuvette, blank subtracted using the absorption spectra of Milli-Q-water, corrected for instrument-specific biases and inner filter effects, and normalized to Raman units [*Lawaetz and Stedmon*, 2009; *Kothawala et al*., 2014]. Fluorescence spectra were used to calculate the fluorescence index (FI) [*McKnight et al*., 2001] at an excitation wavelength of 370 nm and emission wavelengths of 470 and 520 nm [*Cory et al*., 2010]. Higher values of the FI (>1.4) have been linked to more internally produced DOC, while lower values (<1.4) indicate DOC that is more aromatic and typically of terrestrial origin [*McKnight et al*., 2001]).

All laboratory analyses were conducted within 48 h from sampling, apart from fluorescence analyses that were conducted within 1 week from sampling. Samples were stored at 4°C and darkened until analyzed.

2.4. Photobleaching Rate Modeling

Using the software R3.0.2 [*R Development Core Team*, 2013] and following methods described by *Osburn et al*. [2009] and *Koehler et al*. [2014], we simulated the depth- and wavelength-specific photobleaching as

$$\Psi^{\mathrm{Day}}(z) = \int_{\lambda_{\min}}^{\lambda_{\max}} E_{\mathrm{od}}^{\mathrm{Day}}(\lambda, 0^-)\, a(\lambda)\, e^{-(K_d(\lambda)z)}\, \Phi(\lambda)\, d\lambda \tag{3}$$

where Ψ^{Day} is the daily photobleaching ($m^{-1}\,m^{-3}\,d^{-1}$), z is the depth (m), $\lambda_{\min}$ and $\lambda_{\max}$ are the minimal and maximal wavelengths (nm), $E_{\mathrm{od}}^{\mathrm{Day}}(\lambda, 0^-)$ is the daily integrated downwelling scalar irradiation just below the water surface (mol photons $m^{-2}\,d^{-1}\,nm^{-1}$), K_d is the vertical attenuation coefficient for downward irradiance (m^{-1}), and Φ is the apparent quantum yield (AQY) of photobleaching (m^{-1} mol photons^{-1}).

Clear-sky downwelling irradiance reaching the water-air interface was simulated using the atmospheric radiative transfer model libRadtran version 1.6 [*Mayer et al*., 2011] and corrected for attenuation by clouds using total cloud cover data retrieved from the archive of the operational mesoscale analysis system at the Swedish Meteorological and Hydrological Institute [*Häggmark et al*., 2000] and a cloud effect function

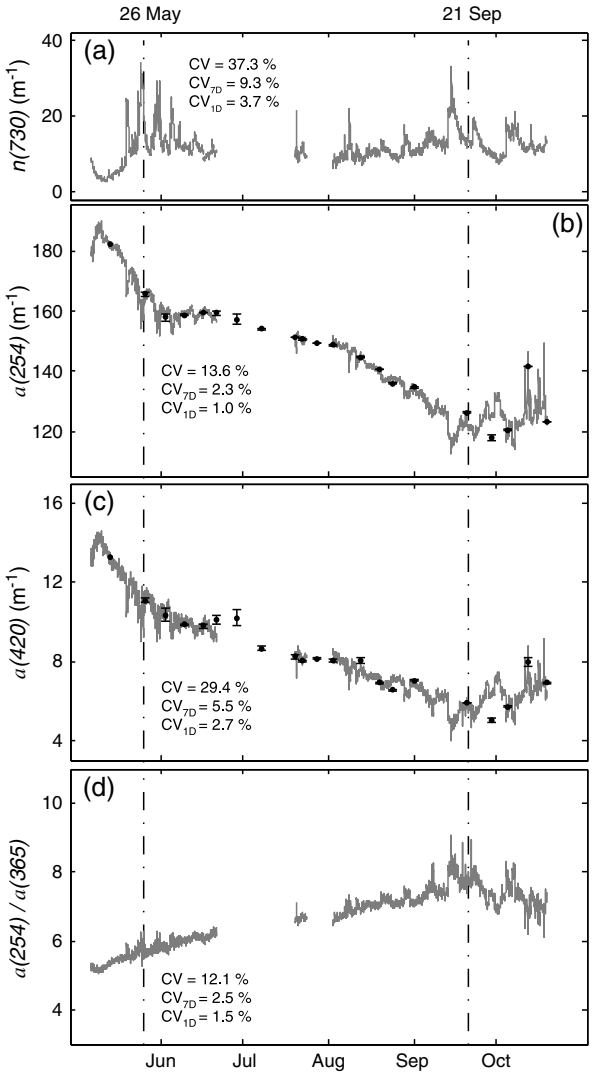

Figure 3. High-frequency in situ spectrophotometer results (30 min intervals, each $N = 6145$) for (a) $n(730)$, (b) $a(254)$, (c) $a(420)$, and (d) the absorption ratio $a(254)/a(365)$. Samples are marked (black dots) with standard deviations (black bars) for $a(254)$ and $a(420)$. For each subfigure, coefficients of variation are given for the complete signal (CV), for signal frequencies higher than the weekly (CV_{7D}), and higher than the daily (CV_{1D}) signal.

[*Kasten and Czeplak*, 1980]. Transmittance into the water body was calculated separately for the diffuse and the direct irradiance fraction, and the just below-water-surface irradiance spectra were converted to scalar irradiance. The simulated cloud-corrected downwelling irradiance reaching the water surface (280 to 600 nm) explained 55% of the variability in the total daily irradiance (300 to 1000 nm) measured by the pyranometer at 1.5 m above the lake. For $a(\lambda)$, and for each sampling occasion ($N = 17$), we used the means of the measured absorption spectra ($N = 3$). K_d was estimated for nine wavelengths between 300 and 400 nm based on linear regression relationships with a and interpolated using an exponential function [*Koehler et al.*, 2014]. We ran two simulations using AQYs of water from Tämnaren (see Text S1 in the supporting information) and lake Tuscaloosa [*Vähätalo and Wetzel*, 2004]. The simulations were conducted for a wavelength range between 280 and 600 nm (1 nm intervals) from just below the water surface with depth steps of 0.005 m down to 0.200 m and with depth steps of 0.050 m down to the mean lake depth averaged between two consecutive sampling dates. Areal photobleaching was calculated by integrating across wavelength and depth using the trapezoid rule. The irradiance and photochemical rate modeling is explained in detail by *Koehler et al.* [2014].

2.5. Regional Comparison

To compare the observed change in specific visible absorption to other lakes in the region, we collected public data from countrywide lake monitoring conducted by the Swedish University of Agricultural Sciences. Data for DOC and $a(420)$ were available for samples ($N = 182$) from 23 lakes that fulfilled the following criteria: lakes were located in similar air temperature zones with mean daily air temperatures above 0°C during 180 ± 20 d yr^{-1}, as delineated by climate maps available at the SMHI (Figure 1a). Samples were from surface waters (0.5 m depth) sampled at least 6 times during the year 2011 and at regular time intervals. To compensate for the differences in means and standard deviations between lakes, we normalized our data by calculating z-scores [*Quinn and Keough*, 2002] for each lake separately.

3. Results

3.1. In Situ High-Frequency Measurements

CDOM peaked around 10 May and declined until 21 September, with an UV absorption loss of >25% for $a(254)$ (Figure 3b) and a visible absorption loss of >50% for $a(420)$ (Figure 3c). The absorption ratio $a(254)/a(365)$ increased during the respective time period by 40% (Figure 3d). Power spectra from the Fourier

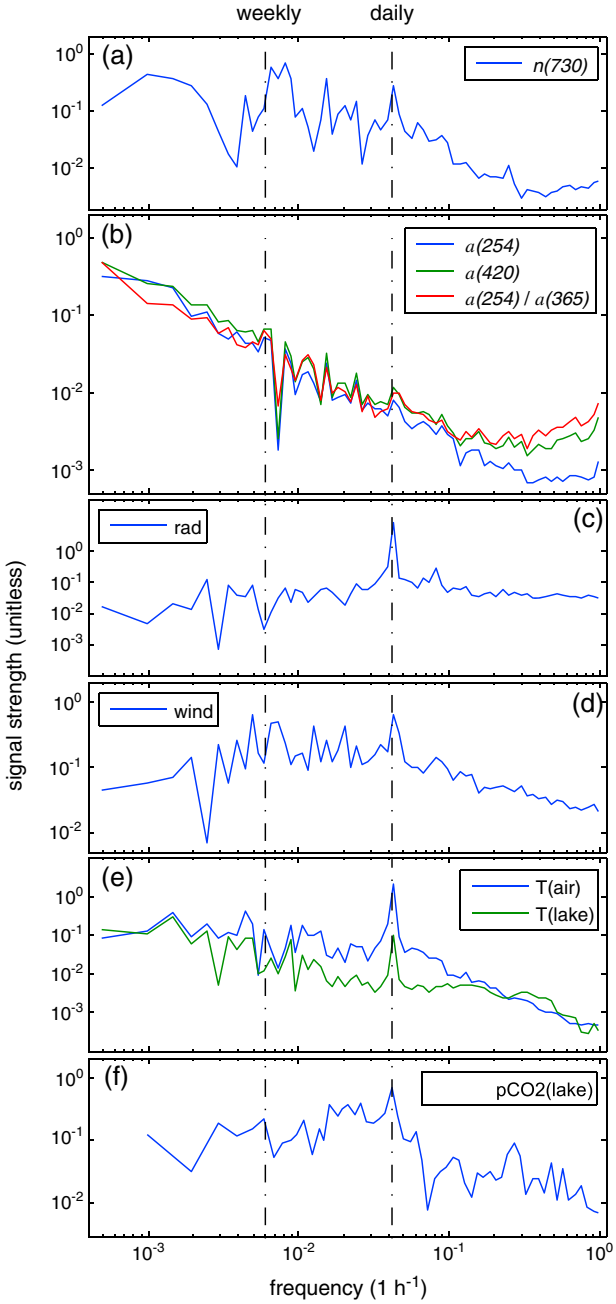

Figure 4. Power spectra from the Fourier analysis for high-frequency in situ spectrophotometer results (a) $n(730)$, (b) $a(254)$, $a(420)$, and the absorption ratio $a(254)/a(365)$, (c) radiation (rad), (d) wind, (e) lake water and air temperatures, and (f) pCO_2 in the lake water. For abbreviations, see Materials and Methods section.

analysis for CDOM absorption metrics $a(254)$, $a(420)$, and $a(254)/a(365)$ showed decreasing signal intensities toward higher frequencies (Figure 4b). For the same metrics, short-term (hourly to daily) signals (CV_{1D} = 1.0 to 2.7%) were roughly 1 magnitude smaller than the temporal variability reported for the complete signals (CVs = 12.1 to 29.4%; Figures 3b and 3c). No regular diurnal pattern could be identified (Figures 5b–5d). Particle interferences $n(730)$ showed abrupt increases at irregular intervals, which thereafter declined over several days (Figure 3a). Accordingly, power spectra from the Fourier analysis disclosed that the temporal signal for $n(730)$ expressed most strongly at daily to weekly time scales (Figure 4a). We found that $n(730)$ showed strong covariation with turbidity levels ($N = 62$, $R^2 = 0.591$, and $P < 0.01$) measured on samples (Figure S2 in the supporting information). Turbidity levels ranged from 13.5 to 48.5 nephelometric turbidity units (NTU). No regular diurnal pattern could be identified for $n(730)$ (Figure 5a).

Power spectra from the Fourier analysis of physical variables (for time series and ranges of the variables, see Figure S3 in the supporting information) showed pronounced diurnal signals for solar radiation, wind, lake water and air temperatures, as well as pCO_2 in the lake water (Figures 4c–4f). Regular reoccurrence of diurnal signals was apparent for diurnal cycles (Figures 5e and 5g–5k), with wind being the exception (Figure 5f). In more detail, solar radiation peaked at noon (12 P.M.); water and air temperatures showed lows in the mornings (6 A.M.) and highs in the afternoon (6 P.M.). Both pCO_2 in the atmosphere, as well as in the lake water, showed minima in the afternoons (6 P.M.) and maxima in the mornings (6 A.M.). Wind speed ranged from near zero to 11.1 m s^{-1} with a mean of 4.0 m s^{-1}.

3.2. Discrete Water Samples

Concentrations of DIC increased gradually from 9.7 mg C L^{-1} to 17.9 mg C L^{-1} during the study period (Figure 6a). Concentrations of DOC varied from 20.1 to 26.2 mg C L^{-1} with a median at 22.5 mg C L^{-1}. Highest DOC values were reported in early July (Figure 6b). Linear relationships between $a(254)$ and DOC ($P < 0.05$ and $R^2 = 0.37$) and $a(420)$ and DOC ($P < 0.05$ and $R^2 = 0.15$) were weak. A rapid loss of specific UV and visible absorption from May to September (−17.1% and −42.5%, respectively; Figures 6c and 6d) was

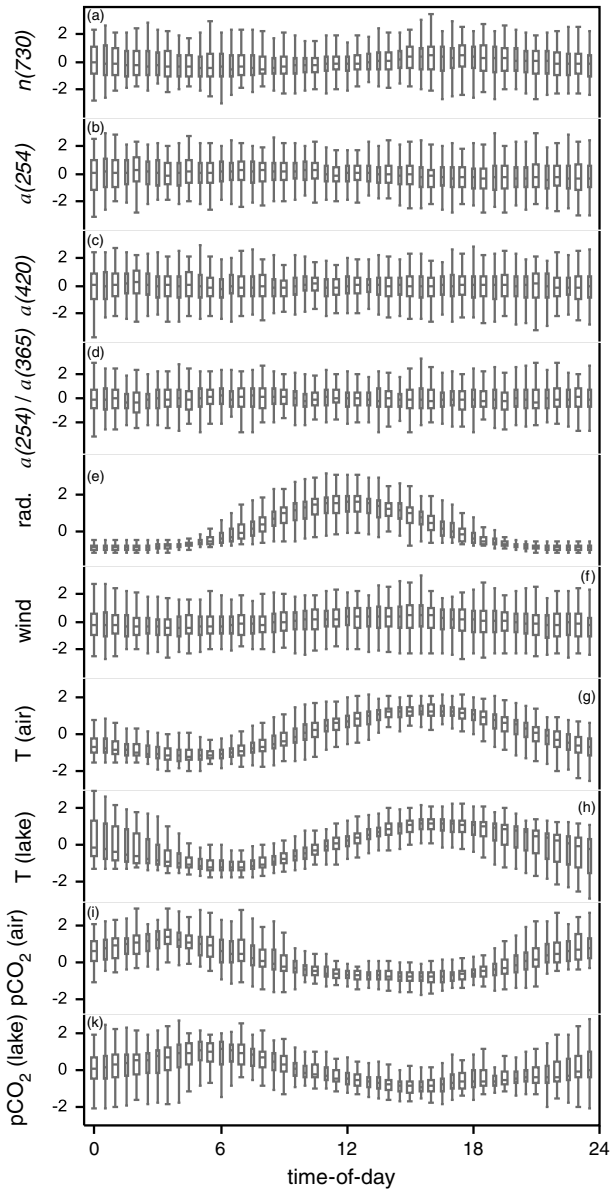

Figure 5. Normalized z-scores for diurnal cycles on a 30 min basis with in situ spectrophotometer results for (a) $n(730)$, (b) $a(254)$, (c) $a(420)$, and (d) the absorption ratio $a(254)/a(365)$. Physical time series for (e) radiation (rad), (f) wind, (g) air and (h) lake water temperatures, and (i) atmospheric pCO_2 and (k) pCO_2 in the lake water. For abbreviations, see Materials and Methods section.

accompanied by increasing (10 to 20%) absorption spectral slopes in the UV-B region (280 to 315 nm) with a maximum increase at 295 nm (Figure 7). Specific UV and visible absorption was regained in October (+17.2% and +44.8%, respectively; Figures 6c and 6d). The strong increase in the fluorescence index (FI from 1.32 to 1.40) during June and early July (Figure 6c) suggests in-lake production of DOC with lower aromatic content [*McKnight et al.*, 2001]. Chl *a* ranged from 11.6 to 72.3 $\mu g\,L^{-1}$ (Figure 6f). In general, spatial variation across sampling sites was low from May to September but high in October: for DOC, $a(254)$ per unit DOC, $a(420)$ per unit DOC, and FI (Figure 6, red bars). The summer loss in specific visible absorption, as $a(420)$ per unit DOC, was also detectable in the regional lake water sampling ($N = 23$), albeit less pronounced compared to the study lake (Figure 8).

3.3. Photobleaching Rate Modeling

Photobleaching rate modeling gave a loss of mean $a(300–700)$ in a similar range to the observed CDOM loss (Table 1): When using the AQY spectrum quantified from Tämnaren lake water (see Text S1 in the supporting information), the simulated photobleaching exceeded the observed summer CDOM loss by roughly 20%. When applying an existing AQY spectrum that had been quantified on the relatively DOC-poor Tuscaloosa reservoir ($DOC < 4\,mg\,C\,L^{-1}$ [*Vähätalo and Wetzel*, 2004]), the simulated CDOM loss fell below the observed CDOM loss by about 28%.

4. Discussion

4.1. Summer CDOM Loss

Our results, based on high-frequency measurements ($N = 6145$, May to October), show a strong gradual CDOM decrease from May to September, which is not interfered by any short-term (subhourly to daily) CDOM variability. Summer CDOM losses as a response of photochemical and biological processes are a well known and a regularly occurring phenomena in boreal lake ecosystems [*Thurman*, 1985; *Miller*, 1998]. For the first time we are able to demonstrate that such CDOM summer losses can exceed subhourly to daily CDOM variability by an order of magnitude over a complete summer period (Figures 3b and 3c). We also detected that the temporal CDOM variability for the UV light wavelength ($a(254)$) strongly covaried with CDOM variability of the visible light wavelength ($a(420)$). Such strong covariations of different wavelengths have previously been observed on a large spatial scale (983 lake systems [*Erlandsson et al.*, 2012]), but they have not been reported on a temporal scale. Despite the strong covariations between UV and visible light

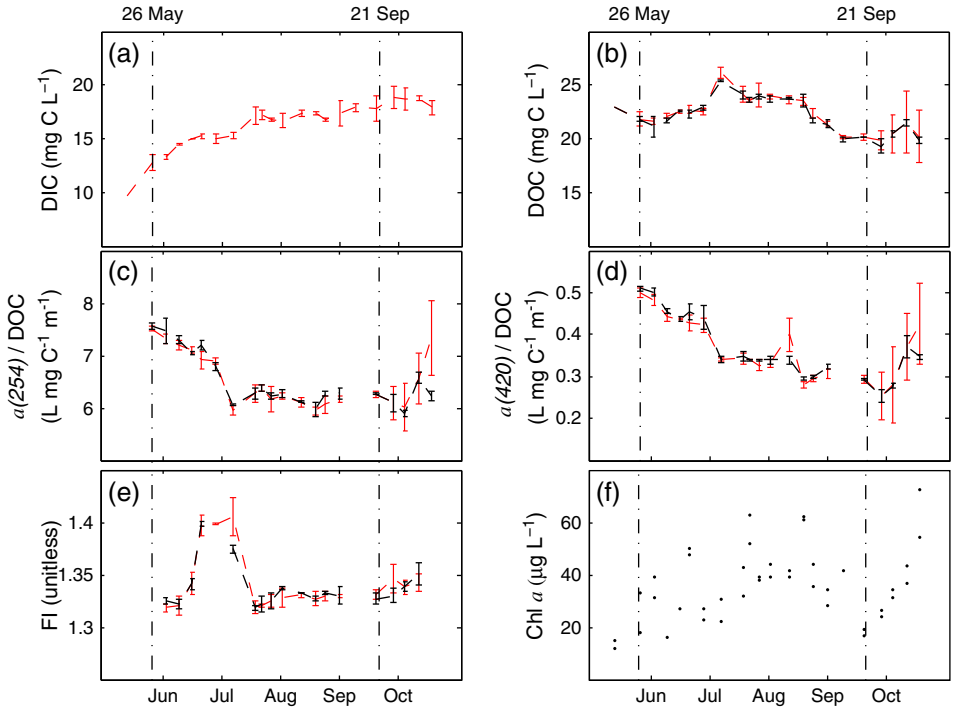

Figure 6. Summary from 21 sampling occasions for (a) dissolved inorganic carbon (DIC), (b) dissolved organic carbon (DOC), (c) specific UV absorption as $a(254)$ per unit DOC, (d) specific visible absorption as $a(420)$ per unit DOC, (e) fluorescence index (FI), and (f) Chl *a*. All figure parts show medians and standard deviations for triplicates taken by the spectrophotometer at the float (black) and for samples taken across the three sampling locations (red) and as marked in Figure 1.

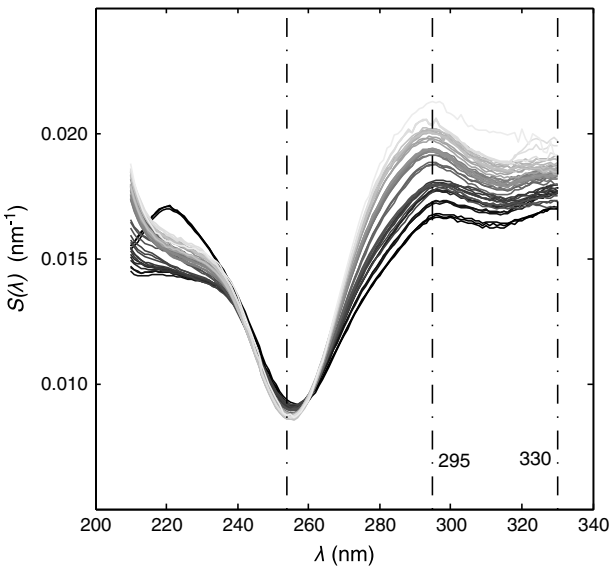

Figure 7. Spectral slope distributions $S(\lambda)$ for absorption spectra measured on filtered samples, which were calculated for 20 nm wavelength bands, at a 1 nm interval and for the wavelength range of 210 to 330 nm following *Loiselle et al.* [2009]. Distributions $S(\lambda)$ are presented for samples collected from 26 May to 21 September, 2011 (dark grey to light grey, respectively).

wavelengths, we still found variations over time in the spectral shape, here estimated by the spectral slope [*Twardowski et al.*, 2004]. Following the methods of *Loiselle et al.* [2009], we were able to localize the strongest increases in absorption spectral slopes $S(\lambda)$ (15 to 20%) throughout summer at a wavelength of 295 nm (Figure 7). Increased $S(\lambda)$ in the UV-B range has been reported for radiation-induced decomposition of CDOM [*Grzybowski*, 2000; *Moran et al.*, 2000; *Yamashita et al.*, 2013]. Since the radiation-induced decomposition of CDOM is known to be among the main drivers for summer CDOM losses [*De Haan*, 1993; *Del Vecchio and Blough*, 2002; *Vähätalo*, 2010], we have a strong indication that the summer CDOM loss in Tämnaren was primarily radiation induced.

Using photochemical rate modeling, we estimated the radiation-induced CDOM loss, generally referred to as photobleaching [*Vähätalo and Wetzel*, 2004]. A modeled CDOM loss of >50% gave

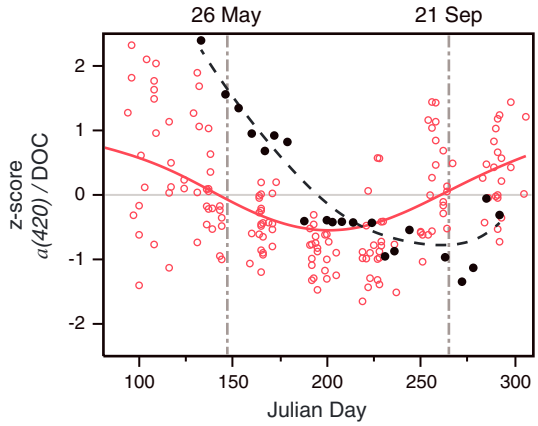

Figure 8. Normalized (z-scores) specific visible absorption as $a(420)$ per unit DOC for samples ($N = 182$) from 23 lakes within the region and in comparison to medians ($N = 21$) from triplicates taken by the spectrophotometer at the float (black dots).

further support for a dominant role of radiation-induced decomposition of CDOM during summer. The estimated CDOM loss exceeded the loss observed in situ by 20%, which may be explained by in-lake production of CDOM or also by residual delivery of terrestrial CDOM from run off during summer. Also, during model parameterization, we assume that the AQY spectrum determined from a single Tämnaren water sample was representative for the photoreactivity throughout summer (see supporting information). Photosensitive CDOM may be effectively consumed at the onset of the season, which increases the proportion of less photoreactive compounds [*Gonsior et al*., 2013], and is one process that may modify the efficiency and shape of the AQY spectrum across a season. While our results indicate that photobleaching is among the main drivers behind the observed summer CDOM loss, we recognize that photochemical rate models require precise definition of AQYs that represent in situ conditions, which is challenging considering the spatial and temporal variability inherent to CDOM [*Miller*, 1998; *Reche et al*., 2000].

Apart from CDOM losses in the UV range, we found even stronger CDOM losses in the visible range. For instance, a CDOM loss of >50% in the visible region (420 nm) exceeded the losses in the UV region (254 nm) by a factor of 2 that resulted in increasing $a(254)/a(365)$ ratios throughout summer (Figure 3b). We argue that higher losses in the visible region and increasing $a(254)/a(365)$ ratios reflect the strong (15 to 20%) increases in spectral slopes observed around 295 nm (Figure 7). In earlier studies, increased $a(254)/a(365)$ ratios have been related to decreases in DOM molecular weights [*De Haan*, 1993; *Dahlén et al*., 1996], as well as increased microbial production [*Berggren et al*., 2007]. We suggest that in Tämnaren, the radiation-induced decomposition of CDOM breaks organic macromolecules into smaller, likely more labile, bioavailable compounds, which may increase microbial activity [*Lindell et al*., 1995; *Wetzel et al*., 1995; *Bertilsson and Tranvik*, 1998]. Assessing the net effect of solar irradiance on microbial activity is however more complex [*Tranvik and Bertilsson*, 2001] and goes beyond the scope of this work.

In addition to the radiation-induced decomposition of CDOM, also other processes can result in CDOM losses during summer months. *Schindler et al*. [1996] found, for example, a reduced delivery of CDOM-rich runoff from terrestrial soils to be characteristic for dry summer months. Other examples of summer CDOM losses include flocculation and subsequent sedimentation of DOC which can selectively remove CDOM from the water column [*von Wachenfeldt and Tranvik*, 2008]. Flocculation may also remove colloidal iron which reduces CDOM [*Köhler et al*., 2013]. Even dilution might result in CDOM decreases, but since DOC

Table 1. Water Depth, Dissolved Organic Carbon (DOC) Concentrations and the Mean CDOM Absorption Coefficient Between 300 and 700 nm $a(300–700)$ Observed at the Beginning (26 May 2011) and End (21 September 2011) of the CDOM Loss Along With the Observed (Δ Observed) and Simulated (Δ Simulated) CDOM Losses for $a(300–700)$

Datum	Depth (m)		DOC (mg C L^{-1})		$a(300 \text{ to } 700)$ (m^{-1})	
26–5–2011	100.0%	1.50	100.0%	21.8	100.0%	17.4
21–9–2011	80%	1.20	92.7%	20.2	60.3%	10.5
Δ observed	−20%	−0.30	7.3%	−1.7	−39.7%	−6.9
Δ simulated (AQY Tämnaren)[a]					−59.2%	−10.3
Δ simulated (AQY Tuscaloosa)[b]					−11.5%	−2.0

[a]Applying the apparent quantum yield from Tämnaren.
[b]Applying the apparent quantum yield from *Vähätalo and Wetzel* [2004].

increased rather than decreased toward summer, we attribute our observed selective CDOM loss to other processes than dilution. Processes typically resulting in decreasing CDOM/DOC ratios toward summer, as observed in Tämnaren as well as in other lakes across Sweden (Figure 8), are photobleaching, flocculation, and in-lake production of DOC [*Erlandsson et al*., 2012; *Guillemette et al*., 2013]. For the productive lake Tämnaren (see section 4.2), we argue that a shift from terrestrial to various in-lake-derived (algae and macrophytes) DOC sources has likely contributed to changing CDOM/DOC ratios [*Jiang et al*., 2012; *Catalán et al*., 2013].

4.2. Short-Term CDOM Variability

While the summer CDOM loss developed steadily from May to September, subhourly to diurnal variability in CDOM was low (CVs = 1.0 to 5.5%; Figures 3b–3d). In general, a low short-term variability for CDOM may be expected in the absence of hydrological flow, since the overall reaction rate is slow [*Koehler et al*., 2012]. Recent high-frequency in situ studies question this assumption, however, and note that short-term CDOM variability is rarely quantified [*Spencer et al*., 2007; *Jennings et al*., 2012]. For lake systems in particular, the timing of in-lake production and the response of CDOM to such are yet unclear [*Coloso et al*., 2011]. Tämnaren was highly productive during the study period, as indicated by Chl *a* levels above 20 $\mu g\,L^{-1}$. A peak in the fluorescence index (FI) in June and early July indicates a period of in-lake DOM production [*McKnight et al*., 2001]. The productive period was followed by the highest DOC concentration (26.2 $mg\,C\,L^{-1}$; 7 July 2011). The pCO_2 in the lake water measured from 24 August to 19 October showed regular diurnal cycles (Figure 5k) that also indicate photosynthetic production. A regular diurnal CDOM signal resulting from photosynthetic production was however not apparent (Figure 5).

Diurnal patterns in CDOM were previously attributed as a response to primary production in a river with low concentration of DOC ($<3.5\,mg\,C\,L^{-1}$) [*Spencer et al*., 2007]. In a previous analysis of lakes with relatively low concentrations of DOC ($<5.5\,mg\,C\,L^{-1}$), CDOM was generally not coupled to short-term variation in lake metabolism [*Coloso et al*., 2011]. Possibly, diurnal patterns could be identified in these cases due to a low background and a high relative importance of indigenous production. We suggest that diurnal patterns in CDOM are often quenched by stronger effects associated with imported CDOM. In boreal areas such as Sweden, the average DOC concentration is generally twice as high (median $>10\,mg\,C\,L^{-1}$) as in the systems where CDOM diurnal dynamics have been demonstrated [e.g., *Erlandsson et al*., 2012], and the input of allochthonous DOC dominates over autochthonous DOC production by 1 to 2 orders of magnitude [*Algesten et al*., 2003]. Apart from the absence of a regularly occurring CDOM signal, it was not until autumn that abrupt changes in CDOM were registered (Figure 6). We suggest that the abrupt changes were due to rainfall-induced (Figure S3 in the supporting information) runoff from land. Autumn leaf fall that initiated at the end of September may also have contributed to CDOM delivery from land as reported from other systems [*Aitkenhead-Peterson et al*., 2003].

4.3. Short-Term CDOM Variability and Particle Interference

Tämnaren is turbid (NTU > 10) and wind exposed with average wind of 4 $m\,s^{-1}$ and occasional gusts of over 10 $m\,s^{-1}$. This leads to surface waves that cause frequent resuspension of particles from the sediments of this shallow, wind-exposed lake. Particles strongly affected the beam attenuation coefficient $c(\lambda)$ of the in situ spectrophotometer probe (Figure 2), producing noise that overlaid the signal from the dissolved organic matter $a(\lambda)$. The separation of particle interferences, $n(\lambda)$, from the absorbance of CDOM, $a(\lambda)$, is wavelength dependent and becomes especially challenging toward the visible region, where the ratio $a(\lambda)/n(\lambda)$ drops far below 1 (Figure 2b). In our study lake, particle interferences limited the applicability of the in situ optical approach to the UV and lower visible region (250 to 420 nm).

Studying the power spectra from Fourier analysis, we were able to disclose that the temporal signal from particle interferences $n(\lambda)$ covaried strongly with physical time series at diurnal to weekly time scales. Examples are covariation with solar radiation, temperature (water and air), and pCO_2 in the water (Figure 3). In a turbid system, $n(\lambda)$ can hardly be separated from $a(\lambda)$ in the upper visible region (>600 nm). Where particle interferences are not properly separated from CDOM signals, a covariation with physical variables may be attributed to CDOM variability by spurious correlations.

4.4. Implication for the Regional and Large Scale

Most CDOM studies have either been performed in oligotrophic waters with high DOC concentrations (humic waters) [e.g., *Erlandsson et al*., 2012] or in eutrophic waters with low DOC concentrations [e.g.,

Spencer et al., 2007]. Depending on the type of water, and the season, the main drivers for CDOM varied, ranging from external to internal drivers [*Spencer et al*., 2007; *Erlandsson et al*., 2012]. Tämnaren however represents a third lake category, i.e., a eutrophic and humic lake, for which we found a strong seasonal CDOM absorption signal (Figure 8). A strong seasonal pattern for CDOM absorption is common for oligotrophic humic lakes of the boreal region [*Thurman*, 1985]. Our results indicate that eutrophic humic lakes can show similar CDOM variation patterns as found in oligotrophic humic lakes. Thus, large-scale models that refer to humic lakes, in general, can most probably also be applied to those that are eutrophic and humic. For these lake types, our results indicate that the temporal CDOM absorption signal and the signal from physical variables (e.g., wind, temperature, and pCO_2 levels) are out of phase (Figure 5). This temporal asynchrony is relevant for physical and lake-metabolism models that include both physical as well as biooptical measurements such as CDOM absorption [e.g., *Coloso et al*., 2011].

5. Summary and Conclusions

We reported here a 25 to 50% CDOM loss that developed gradually from May to September 2011. The summer CDOM loss was substantially faster in the visible light range compared to the UV light range, along with an increasing spectral slope in the UV-B light range (280 to 315 nm). We attribute the continuous increase in the spectral slope in this wavelength range to the radiation-induced decomposition of CDOM that is in accordance with earlier studies addressing radiation-induced CDOM losses for both terrestrial and marine waters [*Grzybowski*, 2000; *Moran et al*., 2000; *Yamashita et al*., 2013]. However, a strong in-lake DOC production was also apparent from sampling and, e.g., expressed in fluorescence measurements (FI) designed to disclose in-lake production of DOC. This lake-internal DOC production was not expressed in any of the CDOM absorption metrics applied, and thereby contrasts studies from less humic surface waters that reported both short-term [*Spencer et al*., 2007] and more irregular [*Coloso et al*., 2011] CDOM responses to in-lake production of DOC.

We conclude that CDOM variability in the shallow, humic, and eutrophic lake Tämnaren was substantially influenced by photochemical degradation of CDOM, which acts differently at different wavelengths. Since the shape of the spectral slope distribution $S(\lambda)$ quantified for Tämnaren samples is typical for humic lake waters [*Loiselle et al*., 2009] our results may be applicable also to other lakes. We suggest that lake-internal CDOM signals are quenched in humic lake waters by effects that associate with CDOM delivery via runoff from land and its subsequent degradation within the lake that we consider to be driven mainly by solar exposure. Accordingly, for humic lake waters, we suggest that changes in CDOM spectral shapes, and a(254)/a(365) ratios, are predictable from solar exposure.

Acknowledgments

This work developed within the research framework "The Color of Water." Direct financial support was received from the Swedish Research Council (VR) and the Swedish Research Council for Environment, Agricultural Sciences, and Spatial Planning (FORMAS). Our work profited from research frameworks established by the European Union (Netlake), the U.S. National Science Foundation (GLEON), the UK Natural Environmental Research Council (CLAD), the Norwegian Research Council (Norklima ECCO), and NordForsk (CRAICC, DOMQUA). We would like to thank Xing Ji and Jan Johansson for their assistance in the laboratory and field, as well as Andreas Andersson for his assistance in the field. We would like to thank Susan Waldron, Don Pierson, and Paul Hanson, for valuable discussions, as well as the two anonymous reviewers for their critical review of the manuscript. To access the data published in this article, refer to the corresponding author.

References

Aitkenhead-Peterson, J. A., W. H. McDowell, and J. C. Neff (2003), Sources, production, and regulation of allochthonous dissolved organic matter inputs to surface waters, in *Aquatic Ecosystems: Interactivity of Dissolved Organic Matter*, edited by S. Findlay and R. Sinsabaugh, pp. 26–70, Academic Press, New York.

Algesten, G., S. Sobek, A. K. Bergstrom, A. Ågren, L. J. Tranvik, and M. Jansson (2003), Role of lakes for organic carbon cycling in the boreal zone, *Global Change Biol.*, *10*(1), 141–147, doi:10.1111/j.1365-2486.2003.00721.x.

Berggren, M., H. Laudon, and M. Jansson (2007), Landscape regulation of bacterial growth efficiency in boreal freshwaters, *Global Biogeochem. Cycles*, *21*, GB4002, doi:10.1029/2006GB002844.

Bertilsson, S., and L. J. Tranvik (1998), Photochemically produced carboxylic acids as substrates for freshwater bacterioplankton, *Limnol. Oceanogr.*, *43*(5), 885–895, doi:10.2307/2839183.

Bertilsson, S., and L. J. Tranvik (2000), Photochemical transformation of dissolved organic matter in lakes, *Limnol. Oceanogr.*, *45*(4), 753–762.

Brunberg, A. K., and P. Blomqvist (1998), Vatten i Uppsala län 1997, *Beskrivning*, *utvärdering*, *åtgärdsförslag*, Upplandsstiftelsen.

Catalán, N., B. Obrador, M. Felip, and J. L. Pretus (2013), Higher reactivity of allochthonous vs. autochthonous DOC sources in a shallow lake, *Aquat. Sci.*, *75*(4), 581–593, doi:10.1007/s00027-013-0302-y.

Coloso, J. J., J. J. Cole, and M. L. Pace (2011), Difficulty in discerning drivers of lake ecosystem metabolism with high-frequency data, *Ecosystems*, *14*(6), 935–948, doi:10.1007/s10021-011-9455-5.

Cory, R. M., M. P. Miller, D. M. McKnight, J. J. Guerard, and P. L. Miller (2010), Effect of instrument-specific response on the analysis of fulvic acid fluorescence spectra, *Limnolo. Oceanogr.Methods*, *8*, 67–78.

Dahlén, J., S. Bertilsson, and C. Pettersson (1996), Effects of UV-A irradiation on dissolved organic matter in humic surface waters, *Environ. Int.*, *22*(5), 501–506, doi:10.1016/0160-4120(96)00038-4.

De Haan, H. (1993), Solar UV-light penetration and photodegradation of humic substances in peaty lake water, *Limnol. Oceanogr.*, *38*(5), 1072–1076.

Del Vecchio, R., and N. V. Blough (2002), Photobleaching of chromophoric dissolved organic matter in natural waters: Kinetics and modeling, *Mar. Chem.*, *78*(4), 231–253.

Dillon, P., and L. Molot (1997), Effect of landscape form on export of dissolved organic carbon, iron, and phosphorus from forested stream catchments, *Water Resour. Res.*, *33*(11), 2591–2600, doi:10.1029/97WR01921.

Downing, B. D., B. A. Bergamaschi, D. G. Evans, and E. Boss (2008), Assessing contribution of DOC from sediments to a drinking-water reservoir using optical profiling, *Lake Reservoir Manage.*, *24*(4), 381–391, doi:10.1080/07438140809354848.

Erlandsson, M., M. N. Futter, D. N. Kothawala, and S. J. Köhler (2012), Variability in spectral absorbance metrics across boreal lake waters, *J. Environ. Monit.*, *14*(10), 2643–2652, doi:10.1039/c2em30266g.

Fee, E. J., R. E. Hecky, S. E. M. Kasian, and D. R. Cruikshank (1996), Effects of lake size, water clarity, and climatic variability on mixing depths in Canadian Shield lakes, *Limnol. Oceanogr.*, *41*(5), 912–920.

Gonsior, M., P. Schmitt-Kopplin, and D. Bastviken (2013), Depth-dependent molecular composition and photo-reactivity of dissolved organic matter in a boreal lake under winter and summer conditions, *Biogeosciences*, *10*(11), 6945–6956, doi:10.5194/bg-10-6945–2013.

Graneli, W., M. Lindell, and L. Tranvik (1996), Photo-oxidative production of dissolved inorganic carbon in lakes of different humic content, *Limnol. Oceanogr.*, *41*(4), 698–706.

Green, S. A., and N. V. Blough (1994), Optical-absorption and fluorescence properties of chromophoric dissolved organic-matter in natural-waters, *Limnol. Oceanogr.*, *39*(8), 1903–1916.

Grzybowski, W. (2000), Effect of short-term sunlight irradiation on absorbance spectra of chromophoric organic matter dissolved in coastal and riverine water, *Chemosphere*, *40*, 1313–1318.

Guillemette, F., S. L. McCallister, and P. A. del Giorgio (2013), Differentiating the degradation dynamics of algal and terrestrial carbon within complex natural dissolved organic carbon in temperate lakes, *J. Geophys. Res. Biogeosci.*, *118*, 963–973, doi:10.1002/jgrg.20077.

Häggmark, L., K. I. Ivarsson, S. Gollvik, and P. O. Olofsson (2000), Mesan, an operational mesoscale analysis system, *Tellus A*, *52*(1), 2–20.

Hargreaves, B. R. (2003), Water column optics and penetration of UVR, in *UV Effects in Aquatic Organisms and Ecosystems*, edited by E. W. Helbling and H. E. Zagarese, pp. 59–105, Royal Society of Chemistry, Cambridge, U. K.

Helms, J. R., A. Stubbins, J. D. Ritchie, E. C. Minor, D. J. Kieber, and K. Mopper (2008), Absorption spectral slopes and slope ratios as indicators of molecular weight, source, and photobleaching of chromophoric dissolved organic matter, *Limnol. Oceanogr.*, *53*(3), 955–969.

Hu, C. M., F. E. Müller-Karger, and R. G. Zepp (2002), Absorbance, absorption coefficient, and apparent quantum yield: A comment on common ambiguity in the use of these optical concepts, *Limnol. Oceanogr.*, *47*(4), 1261–1267.

Jennings, E., S. E. Jones, L. Arvola, P. A. Staehr, E. Gaiser, I. D. Jones, K. C. Weathers, G. A. Weyhenmeyer, C. Y. Chiu, and E. De Eyto (2012), Effects of weather-related episodic events in lakes: An analysis based on high-frequency data, *Freshwater Biol.*, *57*(3), 589–601, doi:10.1111/j.1365-2427.2011.02729.x.

Jeong, J. J., S. Bartsch, J. H. Fleckenstein, E. Matzner, J. D. Tenhunen, S. D. Lee, S. K. Park, and J. H. Park (2012), Differential storm responses of dissolved and particulate organic carbon in a mountainous headwater stream, investigated by high-frequency, in situ optical measurements, *J. Geophys. Res.*, *117*, G03013, doi:10.1029/2012JG001999.

Jiang, G. J., R. H. Ma, S. A. Loiselle, and H. T. Duan (2012), Optical approaches to examining the dynamics of dissolved organic carbon in optically complex inland waters, *Environ. Res. Lett.*, *7*(3), 034014, doi:10.1088/1748-9326/7/3/034014.

Jones, R. I. (1998), Phytoplankton, Primary Production and Nutrient Cycling, in *Aquatic Humic Substances: Ecology and Biogeochemistry*, edited by D. O. Hessen and L. J. Tranvik, pp. 145–175, Springer, Berlin, Heidelberg.

Kasten, F., and G. Czeplak (1980), Solar and terrestrial radiation dependent on the amount and type of cloud, *Sol. Energy*, *24*(2), 177–189.

Kirchner, J. W., X. H. Feng, C. Neal, and A. J. Robson (2004), The fine structure of water-quality dynamics: The (high-frequency) wave of the future, *Hydrol. Processes*, *18*(7), 1353–1359, doi:10.1002/hyp.5537.

Kirk, J. T. (1994), *Light and Photosynthesis in Aquatic Ecosystems*, Cambridge Univ. Press, U. K.

Koehler, B., E. von Wachenfeldt, D. Kothawala, and L. J. Tranvik (2012), Reactivity continuum of dissolved organic carbon decomposition in lake water, *J. Geophys. Res.*, *117*, G01024, doi:10.1029/2011JG001793.

Koehler, B., T. Landelius, G. A. Weyhenmeyer, N. Machida, and L. J. Tranvik (2014), Sunlight-induced carbon dioxide emissions from inland waters, *Global Biogeochem. Cycles*, *28*, 696–711, doi:10.1002/2014GB004850.

Köhler, S. J., D. Kothawala, M. N. Futter, O. Liungman, and L. J. Tranvik (2013), In-lake processes offset increased terrestrial inputs of dissolved organic carbon and color to lakes, *PLoS One*, *8*(8), e70598, doi:10.1371/journal.pone.0070598.

Korshin, G. V., C. W. Li, and M. M. Benjamin (1997), Monitoring the properties of natural organic matter through UV spectroscopy: A consistent theory, *Water Res.*, *31*(7), 1787–1795.

Kothawala, D. N., C. A. Stedmon, R. A. Müller, G. A. Weyhenmeyer, S. J. Köhler, and L. J. Tranvik (2014), Controls of dissolved organic matter quality: Evidence from a large-scale boreal lake survey, *Global Change Biol.*, *20*(4), 1101–1114, doi:10.1111/gcb.12488.

Kritzberg, E. S., and S. M. Ekström (2012), Increasing iron concentrations in surface waters - A factor behind brownification?, *Biogeosciences*, *9*(4), 1465–1478, doi:10.5194/bg-9-1465-2012.

Lawaetz, A. J., and C. A. Stedmon (2009), Fluorescence Intensity Calibration Using the Raman Scatter Peak of Water, *Appl. Spectrosc.*, *63*(8), 936–940.

Lean, D. (1998), Attenuation of solar radiation in humic waters, in *Aquatic Humic Substances: Ecology and Biogeochemistry*, edited by D. O. Hessen and L. J. Tranvik, pp. 109–124, Springer, Berlin, Heidelberg.

Lindell, M. J., W. Graneli, and L. J. Tranvik (1995), Enhanced bacterial-growth in response to photochemical transformation of dissolved organic-matter, *Limnol. Oceanogr.*, *40*(1), 195–199.

Liu, X. H., Y. L. Zhang, Y. Yin, M. Z. Wang, and B. Q. Qin (2013), Wind and submerged aquatic vegetation influence bio-optical properties in large shallow Lake Taihu, China, *J. Geophys. Res. Biogeosci.*, *118*, 713–727, doi:10.1002/jgrg.20054.

Loiselle, S. A., L. Bracchini, A. M. Dattilo, M. Ricci, A. Tognazzi, A. Cózar, and C. Rossi (2009), Optical characterization of chromophoric dissolved organic matter using wavelength distribution of absorption spectral slopes, *Limnol. Oceanogr.*, *54*(2), 590.

Mattson, J. S., C. A. Smith, T. T. Jones, S. M. Gerchako, and B. D. Epstein (1974), Continuous monitoring of dissolved organic-matter by UV-visible photometry, *Limnol. Oceanogr.*, *19*(3), 530–535.

Mayer, B., A. Kylling, C. Emde, U. Hamann, and R. Buras (2011), libRadtran user's guide, published online.

McKnight, D. M., E. W. Boyer, P. K. Westerhoff, P. T. Doran, T. Kulbe, and D. T. Andersen (2001), Spectrofluorometric characterization of dissolved organic matter for indication of precursor organic material and aromaticity, *Limnol. Oceanogr.*, *46*(1), 38–48.

Meili, M. (1992), Sources, concentrations and characteristics of organic matter in softwater lakes and streams of the Swedish forest region, *Hydrobiologia*, *229*(1), 23–41.

Miller, W. L. (1998), Effects of UV radiation on aquatic humus: Photochemical principles and experimental considerations, in *Aquatic Humic Substances: Ecology and Biogeochemistry*, edited by D. O. Hessen and L. J. Tranvik, pp. 125–143, Springer, Berlin, Heidelberg.

Moran, M. A., W. M. Sheldon, and R. G. Zepp (2000), Carbon loss and optical property changes during long-term photochemical and biological degradation of estuarine dissolved organic matter, *Limnol. Oceanogr.*, *45*(6), 1254–1264.

Morris, D. P., H. Zagarese, C. E. Williamson, E. G. Balseiro, B. R. Hargreaves, B. Modenutti, R. Moeller, and C. Queimalinos (1995), The attenuation of solar UV radiation in lakes and the role of dissolved organic carbon, *Limnol. Oceanogr.*, *40*(8), 1381–1391.

Peuravuori, J., and K. Pihlaja (1997), Molecular size distribution and spectroscopic properties of aquatic humic substances, *Anal. Chim. Acta*, *337*(2), 133–149.
Quinn, G. P., and M. J. Keough (2002), *Experimental Design and Data Analysis for Biologists*, Cambridge Univ. Press, New York.
R Development Core Team (2013), *R: A Language and Environment for Statistical Computing*, R Foundation for Statistical Computing, Vienna.
Rasmussen, J., L. Godbout, and M. Schallenberg (1989), The humic content of lake water and its relationship to watershed and lake morphometry, *Limnol. Oceanogr.*, *34*(7), 1336–1343.
Reche, I., M. L. Pace, and J. J. Cole (2000), Modeled effects of dissolved organic carbon and solar spectra on photobleaching in lake ecosystems, *Ecosystems*, *3*(5), 419–432, doi:10.1007/s100210000038.
Saraceno, J. F., B. A. Pellerin, B. D. Downing, E. Boss, P. A. M. Bachand, and B. A. Bergamaschi (2009), High-frequency in situ optical measurements during a storm event: Assessing relationships between dissolved organic matter, sediment concentrations, and hydrologic processes, *J. Geophys. Res.*, *114*, G00f09, doi:10.1029/2009JG000989.
Schindler, D. W., S. E. Bayley, B. R. Parker, K. G. Beaty, D. R. Cruikshank, E. J. Fee, E. U. Schindler, and M. P. Stainton (1996), The effects of climatic warming on the properties of boreal lakes and streams at the Experimental Lakes Area, northwestern Ontario, *Limnol. Oceanogr.*, *41*(5), 1004–1017.
Shapiro, J. (1966), On the Measurement of Ferrous Iron in Natural Waters, *Limnol. Oceanogr.*, *11*(2), 293–298, doi:10.2307/2833434.
Siddiqui, M., G. Amy, and B. Murphy (1997), Ozone enhanced removal of natural organic matter from drinking water sources, *Water Res.*, *31*(12), 3098–3106.
Snucins, E., and J. Gunn (2000), Interannual variation in the thermal structure of clear and colored lakes, *Limnol. Oceanogr.*, *45*(7), 1639–1646.
Spencer, R. G. M., B. A. Pellerin, B. A. Bergamaschi, B. D. Downing, T. E. C. Kraus, D. R. Smart, R. A. Dahlgren, and P. J. Hernes (2007), Diurnal variability in riverine dissolved organic matter composition determined by in situ optical measurement in the San Joaquin River (California, USA), *Hydrol. Processes*, *21*(23), 3181–3189.
Steinberg, C. (2003), *Ecology of Humic Substances in Freshwaters: Determinants From Geochemistry to Ecological Niches*, Springer, Berlin, Heidelberg.
Stull, R. B. (1988), *An Introduction to Boundary Layer Meteorology*, Springer, Berlin, Heidelberg.
Thurman, E. (1985), *Organic Geochemistry of Natural Waters*, Springer, Berlin, Heidelberg.
Tipping, E., H. T. Corbishley, J. F. Koprivnjak, D. J. Lapworth, M. P. Miller, C. D. Vincent, and J. Hamilton-Taylor (2009), Quantification of natural DOM from UV absorption at two wavelengths, *Environ. Chem.*, *6*(6), 472–476, doi:10.1071/en09090.
Tranvik, L. J., and S. Bertilsson (2001), Contrasting effects of solar UV radiation on dissolved organic sources for bacterial growth, *Ecol. Lett.*, *4*(5), 458–463.
Twardowski, M. S., and P. L. Donaghay (2002), Photobleaching of aquatic dissolved materials: Absorption removal, spectral alteration, and their interrelationship, *J. Geophys. Res.*, *107*(C8), 3091, doi:10.1029/1999JC000281.
Twardowski, M. S., E. Boss, J. M. Sullivan, and P. L. Donaghay (2004), Modeling the spectral shape of absorption by chromophoric dissolved organic matter, *Mar. Chem.*, *89*(1–4), 69–88.
Vähätalo, A. (2010), Light, Photolytic Reactivity and Chemical Products, *Biogeochem. Inland Waters*, *37*, 313–326.
Vähätalo, A. V., and R. G. Wetzel (2004), Photochemical and microbial decomposition of chromophoric dissolved organic matter during long (months-years) exposures, *Mar. Chem.*, *89*(1–4), 313–326, doi:10.1016/j.marchem.2004.03.010.
von Wachenfeldt, E., and L. J. Tranvik (2008), Sedimentation in boreal lakes — the role of flocculation of allochthonous dissolved organic matter in the water column, *Ecosystems*, *11*(5), 803–814.
Wallsten, M. (1974), Flygbildstolkning och beskrivning av Tämnarens vegetation, *Svensk Botanisk Tidskrivt*, *68*, 431.
Weishaar, J. L., G. R. Aiken, B. A. Bergamaschi, M. S. Fram, R. Fujii, and K. Mopper (2003), Evaluation of specific ultraviolet absorbance as an indicator of the chemical composition and reactivity of dissolved organic carbon, *Environ. Sci. Technol.*, *37*(20), 4702–4708, doi:10.1021/es030360x.
Wetzel, R. G. (1983), *Limnology*, Saunders, Philadelphia.
Wetzel, R. G., P. G. Hatcher, and T. S. Bianchi (1995), Natural photolysis by ultraviolet irradiance of recalcitrant dissolved organic matter to simple substrates for rapid bacterial metabolism, *Limnol. Oceanogr.*, *40*(8), 1369–1380.
Weyhenmeyer, G. A., Y. T. Prairie, and L. J. Tranvik (2014), Browning of Boreal Freshwaters Coupled to Carbon-Iron Interactions along the Aquatic Continuum, *Plos One*, *9*(2), doi:10.1371/journal.pone.0088104.
Wilhelm, F. M. (2009), Pollution of aquatic ecosystems I, in *Encyclopedia of Inland Waters*, edited by G. E. Likens, pp. 110–119, Academic Press, Oxford, doi:10.1016/b978-012370626-3.00222-2.
Williamson, C. E., D. P. Morris, M. L. Pace, and A. G. Olson (1999), Dissolved organic carbon and nutrients as regulators of lake ecosystems: Resurrection of a more integrated paradigm, *Limnol. Oceanogr.*, *44*, 795–803.
Yamashita, Y., Y. Nosaka, K. Suzuki, H. Ogawa, K. Takahashi, and H. Saito (2013), Photobleaching as a factor controlling spectral characteristics of chromophoric dissolved organic matter in open ocean, *Biogeosciences*, *10*(11), 7207–7217, doi:10.5194/bg-10-7207-2013.